Multiple-wavelength integrated photonic networks based on microring resonator devices

Benjamin A. Small, Benjamin G. Lee, and Keren Bergman

Department of Electrical Engineering, Columbia University, New York, New York 10027, USA
bas@ee.columbia.edu

Qianfan Xu and Michal Lipson

School of Electrical and Computer Engineering, Cornell University, Ithaca, New York 14853, USA
lipson@ece.cornell.edu

Received August 28, 2006; revised November 12, 2006; accepted November 24, 2006; published January 11, 2007 (Doc. ID 74468)

Microring resonator devices implemented on silicon and silicon-on-insulator substrates have a unique potential to be used in high-bandwidth multiple-wavelength integrated photonic networks. A scheme for the wavelength allocation is proposed, and its feasibility is verified experimentally. The important system-level trade-offs that result from the proposed scheme, including those among bandwidth, device footprint, and electrical power consumption, are discussed as well.

OCIS codes: 060.4250, 130.6750, 230.3990.

1. Introduction

Photonic integrated circuits (PICs) have the potential to realize extremely high-bandwidth optical interconnection with micrometer-scale devices, which consume less power and introduce less latency than their contemporary bulk counterparts. In interconnects used between parallel processors in large-scale high-performance computing systems, vast amounts of bandwidth are exchanged between different processing cores. This interconnect or interconnection network is often a serious bottleneck in overall system performance for high-end high-performance computing system applications. Because of the large bandwidth potentially available to microscale and nanoscale integrated photonic systems, these technologies are a promising means of reducing the bottleneck in these systems and others that leverage optical networks [1]. Both chip-to-chip and on-chip applications are well addressed with PIC technology, where in the former, a separate substrate contains the high-bandwidth PIC and in the latter the PIC is monolithically integrated with computing devices.

Optical microcavities, particularly those based on ring resonator structures, exhibit unique properties that are often desirable for PICs [2]. Microring resonators shaped from nanoscale photonic waveguides can be easily fabricated on conventional silicon and silicon-on-insulator (SOI) substrates, with the potential to support complex photonic networks and PICs, such as the one illustrated in Fig. 1 [3].

The following discussion introduces a novel scheme for organizing high-bandwidth multiple-wavelength packets; this scheme is uniquely compatible with the behavior and functionality of microring resonator-based photonic switching elements. Interconnection networks, which can easily leverage these microrings as switching elements, offer significantly more scalability and modularity than simple interconnection buses and point-to-point links [4]. The possible system-level trade-offs of the proposed scheme, especially relating to system footprint and electrical power consumption, are also evaluated in the context of network size and total bandwidth.

1536-5379/07/020112-9/$15.00

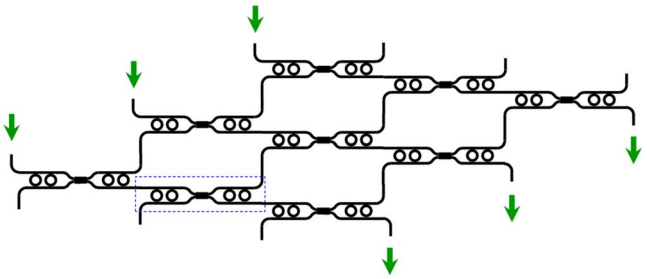

Fig. 1. Conceptual illustration of an augmented 3×3 crossbar network, with a single multiple-wavelength electrically controlled nonblocking switching element highlighted. The coupled waveguides in each switch implement a crossover, and the microring resonators on the same half of the switching elements operate on staggered wavelengths in order to further enhance the bandwidth.

2. Microring Resonator Devices

2.A. Basic Operation

Ring resonators have been demonstrated in a number of platforms for a wide variety of applications. Ring resonators based on conventional optical fiber technology have been used successfully in the implementation of lasers, nonlinear switches, filters, and spectrum analyzers [5–9]. However, these systems are ultimately limited by the size of the bulk optical components, which constrain the network latency, power consumption, and manageability. Microring resonators integrated on semiconductor substrates, including silicon [10], polymers [11], and exotic material systems [12], present scalable and manageable solutions for large high-bandwidth interconnection networks. SOI technology, in particular, provides very high light confinement, allowing smaller bending radii and ultradense integration. Compatibility with existing CMOS fabrication systems and the potential juxtaposition with silicon electronics further increase the appeal of SOI and other silicon-based platforms. Moreover, SOI-based microring devices are able to implement electro-optic modulators [13–15], passive filters [16], and all-optical switches [17].

In the simplest microring structure, a waveguide is coupled to a single ring. When the wavelength of an incident optical signal propagating within the waveguide overlaps a resonant wavelength mode of the ring, the signal can be partially or entirely removed from the waveguide. By simply coupling an additional waveguide to the ring, the extracted resonant modes can be recovered in the secondary waveguide (Fig. 2). This functionality is particularly well suited for filtering and switching both WDM optical signals and multiple-wavelength optical packets. Even more complex photonic structures can be realized by coupling sequences and arrays of rings in various geometries including coupled-resonator optical waveguides (CROW) [18] and side-coupled integrated spaced sequences of resonators (SCISSOR) [19]. Multiple-ring structures such as these allow the transmission shape and dispersion properties of microring-based filters to be tailored [20,21]. Network transmission components have been suc-

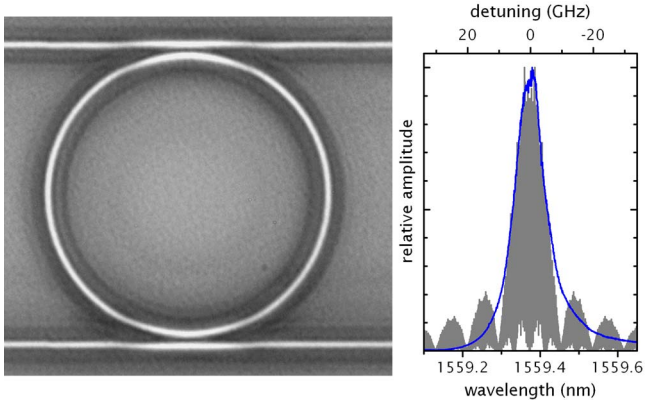

Fig. 2. Left, micrograph of a microring resonator device with both through and drop ports accessible. Right, plot of resulting transmission spectrum for drop port, with the Fourier spectrum for an ideal 10 Gbit/s NRZ-modulated pseudorandom binary sequence signal superimposed.

cessfully fabricated [22], and interesting network architectures for wavelength-selective routing based on these ideas have been envisioned [23,24].

2.B. Bandwidth Limitation

As single-channel data rates increase in high-bandwidth systems, the spectral width of each channel broadens. When these high-speed optical signals pass through devices with narrow transmission spectra, the signals can be distorted quite severely. As high-speed non-return-to-zero (NRZ) on-off-keying optical data signals pass through high-Q microring resonators, distortion occurs due to the nonuniform attenuation of the modulation sidebands (Fig. 2). Even when the carrier wavelength is aligned precisely with the resonance peak, an optical signal's high-frequency components can be greatly attenuated by the resonator's low-pass characteristics, causing smoothing and pulse broadening in the time domain. The authors have previously shown that, as a direct result of this degradation, a power penalty is incurred on an optical signal passing through a resonator; this effect has been analyzed with both experimental results and numerical simulations [25–27]. As the ratio of the optical signal data rate (in gigabits per second) to the resonator FWHM (in gigahertz) increases, the degradation becomes more severe, causing higher power penalties.

2.C. Electro-optic Switches

In addition to passive wavelength filters, modulators and switches can also be implemented by using active devices where the wavelength of the resonant modes can be altered by a small amount. For electro-optic control, typically a p-i-n or MOS structure is embedded around the waveguide; these approaches essentially create a large semiconductor capacitor that can introduce electrons and holes to the waveguide. By manipulating the carrier density of the waveguide, the refractive index is altered because of the free-carrier plasma dispersion effect, thereby shifting the wavelength of the resonant modes. Experimentally, this change in the index of refraction Δn is quantified as

$$\Delta n = -0.8 \times 10^{-3}(\Delta N)^{1.05},$$

$$\Delta n = -2.1 \times 10^{-3}(\Delta P)^{0.8}, \tag{1}$$

for silicon, over the range of interest, where ΔN and ΔP are the excess electron and hole concentrations in units of $10^{18} \times \text{cm}^{-3}$, respectively [28,29]. Different configurations of microring resonators can lead to devices that function as modulators and as 1×2 switching elements (Fig. 2). High-speed optical modulation using active silicon microring resonators has been shown at speeds of up to 4.0 Gbit/s NRZ [14,15].

3. Transmission Scheme

The transmission peak of microring resonator devices is generally very narrow as a result of the high cavity Q required in order to manifest interesting physical properties, as discussed above. Since a high Q implies a narrow resonator transmission band, the modulation rate of high-bandwidth data that can pass through a single resonance peak is limited [25–27]. Instead, utilizing wavelength channels that correspond to resonator modes, the periodicity of which is defined as the free spectral range (FSR), can allow for a significant improvement in total throughput bandwidth, especially for WDM systems with either independently routed wavelength channels or multiple-wavelength packets that traverse a system as a cohesive unit. Therefore it may be advantageous to design microrings with smaller FSRs so that many wavelength channels, each on a particular resonant mode of the ring, may be switched or filtered simultaneously (Fig. 3). Furthermore, multiple adjacent wavelength channels can be collected within a single resonant mode to utilize the resonator bandwidth more efficiently.

Separating signal wavelengths by a resonator FSR has been investigated in the past for wavelength conversion in both III–V and silicon-based material systems [17,30,31]. In the proposed scheme, FSR-spaced signals are leveraged as a means of obtaining higher bandwidth throughputs while using a single resonator device. It is a concern that, for high-bandwidth on-chip photonic networks and PICs, nonlinearities can be detrimental to performance. Although two-photon and free-carrier absorption,

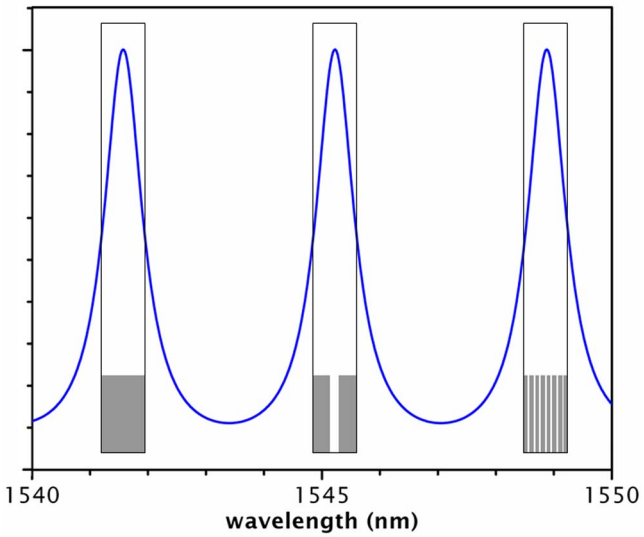

Fig. 3. Conceptual representation of the proposed high-bandwidth transmission scheme. The blue curve represents the multiple-FSR transmission spectrum of a microring resonator device. Open rectangles delimit the spectral range available for the proposed multiple-wavelength transmission format. Within each resonance peak, the spectral range can be partitioned further: gray rectangles correspond to (left) one 100 Gbit/s wavelength, (center) two 40 Gbit/s wavelengths, and (right) eight 10 Gbit/s wavelengths.

Kerr nonlinearities, and the Raman effect can be leveraged for interesting all-optical devices in silicon, high power levels (>10 mW) are typically required [17,31–34]. However, with the power levels typical for communications systems (~50 μW), nonlinearities are rarely manifested [31,32]. The following experimental investigation confirms that transmission with high signal quality can be easily obtained for operation in the regime typical for high-bandwidth networks.

4. Experimental Demonstration

First the power penalty is measured for a single wavelength (1559.34 nm) passing through the microring device; the entire power penalty for this case is due to the nonuniform attenuation of the modulation sidebands by the resonator transmission spectrum, as demonstrated in Refs. [25,26]. Then the same wavelength is transmitted through the ring along with a second wavelength (1546.16 nm), spaced one FSR lower. In this case any additional power penalty would be attributed to cross talk between the two wavelengths, due to nonlinear processes or due to linear effects such as coherent cross talk. However, the following experiment shows no significant additional power penalty.

A microring resonator with a Q of 18,000 was fabricated on an SOI substrate by using strip waveguides with dimensions of 450 nm × 250 nm; it consists of two waveguides coupled to a ring so that both the through and drop ports are accessible (Fig. 2). The two wavelengths, which are modulated independently by a $2^{31}-1$ pseudorandom binary sequence at 10 Gbit/s, are multiplexed onto a single fiber with a 3 dB directional coupler, and the signals are introduced onto the chip by using a tapered fiber and a nanotapered waveguide [35]. Once on chip, the light is transmitted through an SOI waveguide, where it passes through a number of bends before entering the resonator device. The light egresses from either the through port or the drop port of the microring. After exiting the chip, it is collected by another fiber; a polarizer ensures that only the TE mode is used. The optical signals then pass through an erbium-doped fiber amplifier (EDFA), a tunable filter, and a variable optical attenuator. Some of the light is extracted for power measurements, while the rest is detected by a high-speed optical receiver. Polarization controllers are used throughout the setup to provide consistent results with the many polarization-sensitive components. The electronic data signals that are used to drive the modulators are generated from a pulse pattern generator (PPG), and the received electronic signal is analyzed by an oscilloscope and a bit error rate tester (BERT) that is synchronized to

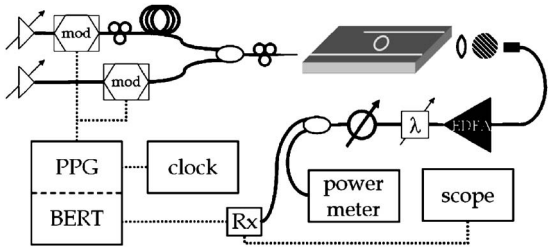

Fig. 4. Schematic of experimental setup, which contains two wavelength channels at the input and an erbium-doped fiber amplifier, tunable filter, and tunable attenuator at the output before a high-speed receiver (Rx).

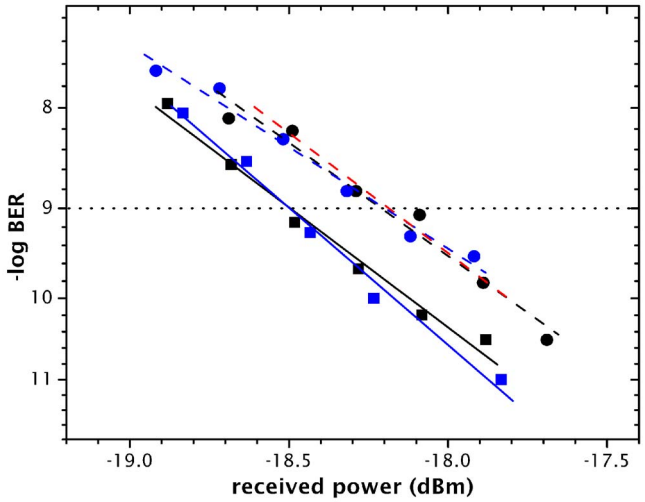

Fig. 5. Bit-error rate curves for the single-channel case (black) and the two-channel case (blue), with back-to-back measurements (squares, solid lines) taken from the through port and device measurements (circles, dashed lines) taken from the drop port, accompanied by the numerically predicted result (red), as from Refs. [25–27].

the pulse pattern generator (Fig. 4). The effects of the narrowband transmission characteristics are investigated by setting the tunable laser to wavelengths within the resonance band (centered at 1559.38 nm), so that the signal passes through the drop port of the microring. To isolate these effects, measurements are also taken off resonance (~1558 nm), so that the signal egresses from the through port and is unaffected by the resonance characteristics.

The power penalty curves for the two situations are nearly identical, and the variance between the two is certainly smaller than the experimental uncertainty (Fig. 5). Furthermore, the resulting power penalty value of 0.29 ± 0.01 dB agrees with the numerical simulations, as detailed in Refs. [25,26]. This result confirms that two wavelengths on different FSRs of the same microring resonator experience negligible cross talk, and no effects are observed that would limit the practicability of systems based on the proposed technique. Microring-based network architectures that leverage this multiple-wavelength scheme, especially when designed to accommodate multiple-FSR transmission, will have the capacity for high total bandwidth.

5. System Architecture

A scheme that takes advantage of this ability to transmit multiple channels separated by multiples of the FSR through the same microring resonator devices is proposed. The accompanying network architectures are comprised of photonic switches that contain multiple microrings, each responsible for routing a set of FSR-separated channels. The augmented 3×3 crossbar network given in Fig. 1 is an example comprising nine of these complete electrically controlled 2×2 multiple-wavelength switches. The proposed noninterfering, nonblocking switches consist of four microrings, two of which are responsible for routing a single input port. By having two rings for each port, two separate FSR-spaced channel groups can be switched independently or simulta-

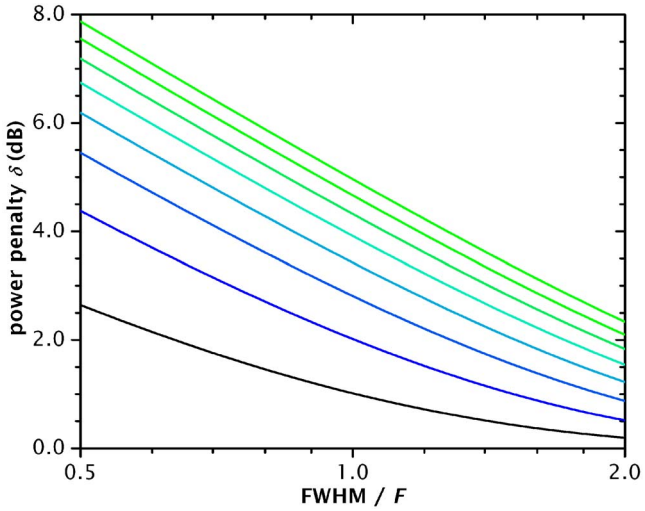

Fig. 6. Plots of power penalty versus the ratio of FWHM (in gigahertz) to modulation frequency F (in gigabits per second), for a single microring resonator (black) and cascades of two through eight microrings (blue to green), obtained from the numerical model discussed in Ref. [27].

neously. Any microring-based topology can be modified to accommodate the proposed high-bandwidth multiple-wavelength transmission scheme based on multiple-FSR utilization, e.g., see Refs. [22,23].

5.A. Power Penalty and Attenuation

The first important system-level considerations for microring resonator-based interconnection networks are the power penalty and insertion loss introduced by each of the switching elements. As first introduced in Refs. [25,26], the power penalty experienced by a high-speed optical signal as it passes through a narrow filter or resonator-based switching element is related to Q (resonator quality factor). References [25–27] elaborate on the methodology used for these numerical simulations, which are based on conventional Fourier analysis. The power penalty accumulates with each successive device and is even more significant for narrower resonances or higher-channel bandwidths (Fig. 6). Furthermore, even microring resonators with ideal coupling coefficients necessarily attenuate incident optical signals. While signals that exit the through port of a device (off resonance) experience negligible attenuation, those that exit the drop port (on resonance) experience insertion loss dominated by a component that is proportional to $1/Q$, assuming near-critical coupling, where Q can be divided into two terms by $1/Q=1/Q_0+1/Q_c$, with Q_0 and Q_c, respectively, the intrinsic and coupling contributions [36]. This insertion loss accumulates with every cumulative cascaded resonator device.

Therefore both power penalty and attenuation grow with the number of microrings traversed in a PIC network. Fortunately, for most interconnection network topologies, the number of devices encountered by a particular signal is logarithmically proportional to the total number of network input and output ports [4]. Nevertheless, there is a critical design trade-off between the size of a network and the allowable signal degradation.

5.B. Footprint

In SOI technology, the FSR of a ring within the C band (1529–1577 nm) can be approximated by its radius R:

$$\mathrm{FSR}=\frac{\lambda_0^2}{2\pi n_{\mathrm{eff}}R}\approx\frac{670\ \mathrm{nm}\ \mu\mathrm{m}}{2\pi R}. \tag{2}$$

To achieve higher-bandwidth devices, the FWHM of each resonance can be increased (lower Q) to allow more data per channel, or the FSR can be reduced so that more bands of channels can be fitted over the spectral range. In the former case, where the Q of the microrings is lower, switching and extinction ratios are often very poor [14,15,17,25–27]. However, this problem can be avoided by maintaining high Q values

while reducing the FSR, although insertion loss may be augmented further. The number of FSR bands available over the C band can also be approximated by the ring diameter

$$N_{\mathrm{FSR}} = \frac{2\pi n_{\mathrm{eff}} \Delta\lambda R}{\lambda_0^2} \approx \frac{2\pi}{14\ \mu\mathrm{m}} R, \tag{3}$$

again assuming typical SOI waveguides. This result has the unfortunate implication that, in order to allow for greater transmission capacity, larger microring resonators must be used. There is therefore a clear trade-off between device footprint and network bandwidth.

5.C. Power Consumption

As mentioned above, active devices based on microring resonators are modulated by introducing carriers via a p-i-n structure or semiconductor capacitor, which changes the index of refraction of the waveguides and thus shifts the resonant wavelength. Driving these large p-i-n diodes requires power that is proportional to the area of the device and to the switching speed. The previous subsection discusses the trade-off between device size and transmission capacity, and this can be extended to the electrical power consumption of the network. To allow more FSRs into the C band, device size must be increased; but larger devices require proportionally more power to modulate and switch.

The first implementations and prototypes of the microring-based electro-optic switch are dominated by the contact resistance and parasitic capacitances. When this technology matures, the switching power will approach the minimum required for driving carriers into the waveguide and producing the required index change. To attain a typical 20 dB switching ratio, the required index change has been estimated to be of the order of 4×10^{-4}, independent of the size of the microring, for Q on the order of 15,000 [29]. Thus, by Eqs. (1), the required carrier concentration is of the order of 5×10^{17} cm^{-3} electrons or 1×10^{17} cm^{-3} holes. At such low carrier concentrations, the p-i-n junction needs to be only about 10 μm thick (depth) under normal conditions, and power consumption is dominated by carrier-induced conductivity modulation rather than any of the capacitance components [37]. The ideal power consumption can thus be estimated as a function of the diode width, which is approximately $2\pi R$ for a microring of radius R, relatively independent of modulation frequency over the megahertz and gigahertz range:

$$P_{\mathrm{RF}} \approx p \times 2\pi R, \tag{4}$$

where p is the constant of proportionality. For an ideal silicon p-i-n diode, p is generally of the order of 0.6 μW/μm [37]. For a typical ring of radius 5 μm, this ideal power consumption is calculated to be approximately 19 μW. Although the total power consumption for the prototype generation of these switches is of the order of 1 mW, it has been predicted that straightforward fabrication advances can lead to $p=3$ μW/μm, or $\sim$100 μW for a typical microring [14].

Whereas electronic circuitry requires individual switching elements for each data channel, multiple-FSR devices can switch numerous channels simultaneously. This feature of high-bandwidth PIC interconnection networks is what makes them so attractive: without additional power consumption, multiple high-bandwidth optical channels can be switched by driving a single device. Although optimizing power and bandwidth trade-offs can be complex, the proposed multiple-FSR transmission scheme greatly enhances the switching capacity of microring resonator-based photonic interconnection networks.

6. Conclusions

A new scheme for multiple-wavelength transmission, which takes advantage of the multiple-resonance characteristics of microring resonator-based switching elements, has been proposed and experimentally demonstrated for the first time to our knowledge. By setting wavelength channels on each FSR-separated resonance of a microring, the bandwidth capacity available to an interconnection network can be enhanced immensely. The design of architectures that leverage silicon microrings as switching and routing elements must consider some important trade-offs between optical trans-

mission bandwidth, electrical power consumption, and on-chip network footprint. These high-bandwidth networks are a prime example of the advantages of PICs and are ideal for meeting the demands of state-of-the-art computing systems.

Acknowledgments

K. Bergman, B. A. Small, and B. G. Lee acknowledge the support of the National Science Foundation (NSF) under grant CCF-0523771 and the U.S. Department of Defense under subcontract B-12-664. M. Lipson and Q. Xu acknowledge support from the Cornell Center for Nanoscale Systems, supported by the NSF, and the Interconnect Focus Center Research Program at Cornell University, supported in part by the Microelectronics Advanced Research Corporation (MARCO), its participating companies, and DARPA.

References and Links

1. D. A. B. Miller, "Rationale and challenges for optical interconnects to electronic chips," Proc. IEEE **88**, 728–748 (2000).
2. K. J. Vahala, "Optical microcavities," Nature **424**, 837–846 (2003).
3. M. Lipson, "Guiding, modulating, and emitting light on silicon—challenges and opportunities," J. Lightwave Technol. **23**, 4222–4238 (2005).
4. W. J. Dally and B. Towles, *Principles and Practices of Interconnection Networks* (Morgan Kaufmann, 2004).
5. J. E. Bowers, S. A. Newton, W. V. Sorin, and H. J. Shaw, "Filter response of single-mode fibre recirculating delay lines," Electron. Lett. **18**, 110–111 (1982).
6. L. F. Stokes, M. Chodorow, and H. J. Shaw, "All-single-mode fiber resonator," Opt. Lett. **7**, 288–290 (1982).
7. S. Tai, K. Kyuma, and T. Nakayama, "Novel measuring method for spectral linewidth of laser diodes using fibre-optic ring resonator," Electron. Lett. **21**, 91–93 (1985).
8. K. Iwatsuki, H. Okamura, and M. Saruwatari, "Wavelength-tunable single-frequency and single-polarization Er-doped fibre ring laser with 1.4 kHz linewidth," Electron. Lett. **26**, 2033–2035 (1990).
9. J. E. Heebner and R. W. Boyd, "Enhanced all-optical switching by use of a nonlinear fiber ring resonator," Opt. Lett. **24**, 847–849 (1999).
10. J. Bismuth, P. Gidon, F. Revol, and S. Valette, "Low-loss ring resonators fabricated from silicon based integrated optics technologies," Electron. Lett. **27**, 722–724 (1991).
11. Y. Hida, S. Imamura, and T. Izawa, "Ring resonator composed of low loss polymer waveguides at 1.3 μm," Electron. Lett. **28**, 1314–1316 (1992).
12. D. Rafizadeh, J. P. Zhang, R. C. Tiberio, and S. T. Ho, "Propagation loss measurements in semiconductor microcavity ring and disk resonators," J. Lightwave Technol. **16**, 1308–1314 (1998).
13. L. Zhou and A. W. Poon, "Silicon electro-optic modulators using p-i-n diodes embedded 10-micron-diameter microdisk resonators," Opt. Express **14**, 6851–6857 (2006).
14. Q. Xu, B. Schmidt, S. Pradhan, and M. Lipson, "Micrometre-scale silicon electro-optic modulator," Nature **435**, 325–327 (2005).
15. Q. Xu, B. Schmidt, J. Shakya, and M. Lipson, "Cascaded silicon micro-ring modulators for WDM optical interconnection," Opt. Express **14**, 9430–9435 (2006).
16. B. E. Little, J. S. Foresi, G. Steinmeyer, E. R. Thoen, S. T. Chu, H. A. Haus, E. P. Ippen, L. C. Kimerling, and W. Greene, "Ultra-compact Si–SiO2 microring resonator optical channel dropping filters," IEEE Photon. Technol. Lett. **10**, 549–551 (1998).
17. V. R. Almeida, C. A. Barrios, R. R. Panepucci, and M. Lipson, "All-optical control of light on a silicon chip," Nature **431**, 1081–1084 (2004).
18. A. Yariv, Y. Xu, R. K. Lee, and A. Scherer, "Coupled-resonator optical waveguide: a proposal and analysis," Opt. Lett. **24**, 711–713 (1999).
19. J. E. Heebner, R. W. Boyd, and Q.-H. Park, "SCISSOR solitons and other novel propagation effects in microresonator-modified waveguides," J. Opt. Soc. Am. B **19**, 722–731 (2002).
20. J. V. Hryniewicz, P. P. Absil, B. E. Little, R. A. Wilson, and P.-T. Ho, "Higher order filter response in coupled microring resonators," IEEE Photon. Technol. Lett. **12**, 320–322 (2000).
21. C. J. Kaalund and G.-D. Peng, "Pole-zero diagram approach to the design of ring resonator-based filters for photonic applications," J. Lightwave Technol. **22**, 1548–1559 (2004).
22. A. Agarwal, P. Toliver, R. Menendez, S. Etemad, J. Jackel, J. Young, T. Banwell, B. E. Little, S. T. Chu, W. Chen, W. Chen, J. Hryniewicz, F. Johnson, D. Gill, O. King, R. Davidson, K. Donovan, and P. J. Delfyett, "Fully programmable ring-resonator-based integrated photonic circuit for phase coherent applications," J. Lightwave Technol. **24**, 77–87 (2006).
23. R. S. Soref and B. E. Little, "Proposed *N*-wavelength *M*-fiber WDM crossconnect switch using active microring resonators," IEEE Photon. Technol. Lett. **10**, 1121–1123 (1998).
24. B. E. Little, S. T. Chu, W. Pan, and Y. Kokubun, "Microring resonator arrays for VLSI photonics," IEEE Photon. Technol. Lett. **12**, 323–325 (2000).
25. B. A. Small, B. G. Lee, K. Bergman, Q. Xu, J. Shakya, and M. Lipson, "High data rate signal integrity in micron-scale silicon ring resonators," in *Proceeding of the Conference on Lasers and Electro-Optics* (Optical Society of America, 2006), paper CTuCC4.

26. B. G. Lee, B. A. Small, K. Bergman, Q. Xu, and M. Lipson, "Transmission of high-data-rate optical signals through a micrometer-scale silicon ring resonator," Opt. Lett. **31**, 2701–2703 (2006).
27. B. A. Small, B. G. Lee, and K. Bergman, "On cascades of resonators for high-bandwidth integrated optical interconnection networks," Opt. Express **14**, 10811–10818 (2006).
28. R. A. Soref and B. R. Bennett, "Electrooptical effects in silicon," IEEE J. Quantum Electron. **23**, 123–129 (1987).
29. S. J. Emelett and R. Soref, "Design and simulation of silicon microring optical routing switches," J. Lightwave Technol. **23**, 1800–1807 (2005).
30. P. P. Absil, J. V. Hryniewicz, B. E. Little, P. S. Cho, R. A. Wilson, L. G. Joneckis, and P.-T. Ho, "Wavelength conversion in GaAs micro-ring resonators," Opt. Lett. **25**, 554–556 (2000).
31. C. Manolatou and M. Lipson, "All-optical silicon modulators based on carrier injection by two-photon absorption," J. Lightwave Technol. **24**, 1433–1439 (2006).
32. E. Dulkeith, Y. A. Vlasov, X. Chen, N. C. Panoiu, and R. M. Osgood, "Self-phase-modulation in submicron silicon-on-insulator photonic wires," Opt. Express **14**, 5524–5534 (2006).
33. R. L. Espinola, J. I. Dadap, R. M. Osgood, Jr., S. J. McNab, and Y. A. Vlasov, "Raman amplification in ultrasmall silicon-on-insulator wire waveguides," Opt. Express **12**, 3713–3718 (2004).
34. Ö. Boyraz, P. Koonath, V. Raghunathan, and B. Jalali, "All optical switching and continuum generation in silicon waveguides," Opt. Express **12**, 4094–4102 (2004).
35. V. R. Almeida, R. Panepucci, and M. Lipson, "Nanotaper for compact mode conversion," Opt. Lett. **28**, 1302–1304 (2003).
36. A. Yariv, "Critical coupling and its control in optical waveguide-ring resonator systems," IEEE Photon. Technol. Lett. **14**, 483–485 (2002).
37. R. H. Caverly and G. Hiller, "The frequency-dependent impedance of p-i-n diodes," IEEE Trans. Microwave Theory Tech. **37**, 787–790 (1989).